Journal of Photochemistry & Photobiology, B: Biology 210 (2020) 111959

Contents lists available at ScienceDirect

Journal of Photochemistry & Photobiology, B: Biology

journal homepage: www.elsevier.com/locate/jphotobiol

Neurite growth of trigeminal ganglion neurons *in vitro* with near-infrared light irradiation

Heejoo Cho[a], Hee-Jae Jeon[a], Seonho Park[a], Chul-Seung Park[b], Euiheon Chung[a,*]

[a] Department of Biomedical Science and Engineering, Gwangju Institute of Science and Technology (GIST), Gwangju 61005, Republic of Korea
[b] School of Life Sciences, Gwangju Institute of Science and Technology (GIST), Gwangju 61005, Republic of Korea

ARTICLE INFO

Keywords:
Primary cell culture
Photobiomodulation
Trigeminal ganglion neuron
Near-infrared light
Laser modulation mode (pulsed wave, continuous wave)

ABSTRACT

Trigeminal ganglion (TG) neurons play an essential role in the sensory nerves of the face. Damaged TG neurons resulting from the accidental and non-intentional nerve lesions, commonly identified as neuropathic pain, which is known to cause intense pain and sensory abnormalities. For the treatment, surgical methods are conducted when the pharmacological treatment fails to provide satisfactory recovery. However, the process of surgery or drug intake can burden the patient or cause side effects. One of the logical choices of study becomes photobiomodulation (PBM) referred to as therapeutic approaches based on the interactions of visible or near-infrared (NIR) photons with biomolecules inside cells or tissues. In this study, we constructed a PBM illumination setup to stimulate the cultured primary TG neurons and compared the growth morphology between the non-irradiated control group and irradiation group with NIR laser of 808 nm wavelength. In addition, we applied various radiant exposures of 1, 2, and 10 J/cm^2 with different pulse frequencies of 1, 10, and 100 Hz. We found that PBM could promote neurite growth of TG neurons, and it works at relatively low energy densities at 1 and 2 J/cm^2. The irradiation group in the pulsed wave mode with the frequency of 10 Hz was found to be the most effective when compared to other frequencies. Thus, PBM on TG neurons facilitated neuronal growth *in vitro* in a dose and frequency-dependent fashion. PBM may provide a potential therapeutic approach to treat damaged peripheral nerves.

1. Introduction

The primary function of the trigeminal nerve, which is the fifth cranial nerve, is to provide motor and sensory innervations to the face [1]. The trigeminal nerve conveys information through three main divisions, the ophthalmic, the maxillary, and the mandibular divisions. Branches of the trigeminal nerve are frequently damaged as a result of trauma or iatrogenic damage during routine surgical procedures [2,3]. Injury or several diseases (such as stroke, facial injuries, brain tumor, and neurological condition) to trigeminal nerve can cause trigeminal neuralgia with intense pain, cluster headache, dry eye syndrome, and Wallenberg syndrome from a few seconds to several hours [4–6].

The treatment of injured trigeminal nerve depends on the cause. In cases where there are structural compression, the surgical resection of the nerve is a possibility [7–9]. However, because surgery has many associated risks, many cases have been treated pharmacologically before any invasive intervention is attempted. In addition, over time, some people with such conditions may stop responding to medications, or they may experience unpleasant side effects [10]. Thus, there is a need for an alternative method of treatment which is non-invasive and reduces the burden on the patients [11].

In recent years, there has been study about the active peripheral nerve regeneration process that plays a pivotal role in the relief of neuropathic pain [12,13]. The potential treatment methods of clinical utility for peripheral nerve regeneration include the interposition of an artificial nerve scaffold, electrical stimulation, guiding regenerative gel, and laser phototherapy [14]. Among these techniques, considerable interest was in the potential therapeutic value of low-level laser irradiation for peripheral nerve recovery and the preservation of denervated muscles [15]. PBM is known to promote wound healing, treat neurodegenerative disorders [16], reduce inflammation [17], improve hearing [18], and relieve acute or chronic pain from injuries or lesions [19,20]. PBM effect on cells is known to generate photochemical responses mainly in the mitochondria and nucleus [21–25]. Even though there are several studies of peripheral nerve regeneration [26,27], the effect of PBM on TG neurons has not been explored.

Here, we demonstrated that PBM has an effect on the regeneration of primary TG neurons *in vitro* using a transgenic *Thy1*-YFP mouse line.

* Corresponding author.
E-mail address: ogong50@gist.ac.kr (E. Chung).

https://doi.org/10.1016/j.jphotobiol.2020.111959
Received 28 December 2019; Received in revised form 9 March 2020; Accepted 10 July 2020
Available online 15 July 2020
1011-1344/

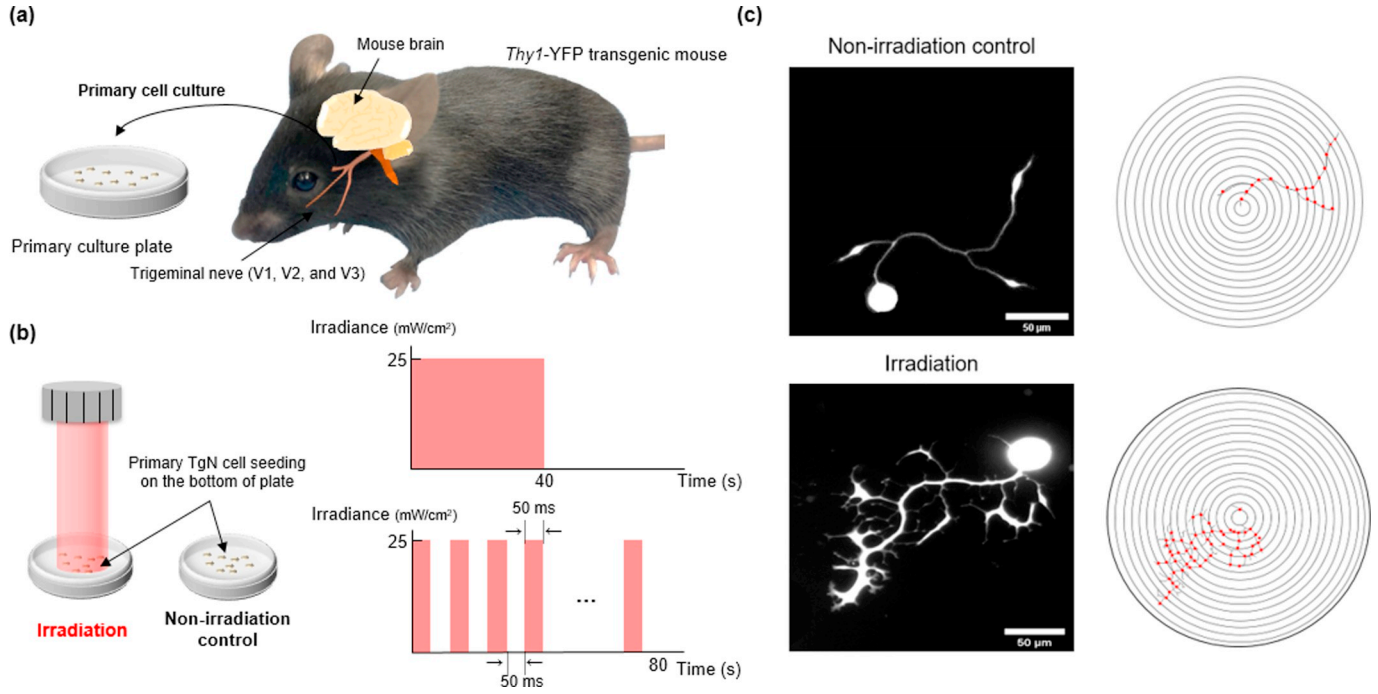

Fig. 1. Schematic diagram of the general concept and strategy for this study. (a) TG neurons harvested from transgenic mice and were seeded on the bottom of the culture plate. (b) We stimulated cultured TG neurons using PBM with a wavelength of 808 nm (irradiance of 25 mW/cm^2, CW and PW mode with 1, 10, and 100 Hz frequency). In the laser diagram, energy density of 1 J/cm^2 and frequency of 10 Hz were used as an example. (c) We measured morphological growth by monitoring TG neurons regeneration image and Sholl analysis between irradiation group and non-irradiation group.

In this study, we quantitatively analyzed the morphological changes of irradiation groups compared with non-irradiation control. We analyzed the neurite length and neurite complexity of TG neurons with respect to the laser mode either continuous wave (CW) or pulsed wave (PW) with an 808 nm NIR laser. In addition, we found optimal parameters of energy density, radiant exposure time, and laser irradiation mode to yield an effective neurite growth for the TG neurons.

2. Materials and Methods

We studied the growth effect of TG neurons by using a NIR laser and measured TG neurons between irradiation and non-irradiation groups using 808 nm laser (CW and PW) as shown in Fig. 1. Our experiment is composed of three main parts: primary cell culture, laser irradiation, and quantitative morphological analysis.

2.1. Animal Care

The handling of animals was conducted strictly according to the recommendations in the guidelines of Institutional Animal Care and Use Committee board (IACUC) of the Gwangju Institute of Science and Technology (GIST), South Korea. The Laboratory Animal Resource Center (LARC) of GIST approved the animal experimental protocol (Protocol Number: GIST-2019-050). The *Thy1*-YFP transgenic mice (Stock No: 003709, Jackson Laboratory, Bar Harbor, ME, USA) with body weight of 20–25 g were used in this study. The experimental animals were housed in the LARC and were maintained under a 12 h light/dark cycle with access to food and water *ad libitum*.

2.2. Primary Cell Culture

Firstly, three mice sample were anesthetized with isoflurane (2–3% with flow rate of 0.5–0.7 l/min). Soon after the mice were decapacitated, the TG neurons were collected from *Thy1*-YFP transgenic mice, rinsed thrice in cold calcium and magnesium-free Hanks' balanced salt solution (HBSS; Invitrogen, Life Technologies, Carlsbad, CA, USA). The isolation procedure was adapted from the protocol of Malin et al. [28]. The TG neurons were minced with a razor blade and incubated at a temperature of 37 °C for a period of 20–30 min filtered papain solution; 53 μl papain (Worthington Biochemical, Lakewood, NJ, USA) to 1 ml Ca^{2+}/Mg^{2+} free HBSS, 1 mg L-Cys (Sigma, St Louis, MO, USA) and 3 μl saturated NaHCO3 (Sigma), and filtered Collagenase/Dispase solution; 0.012 g collagenase type II (Worthington Biochemical) and 0.014 g Dispase type II (Sigma) to 3 ml Ca^{2+}/Mg^{2+} free HBSS was used for the formulation of the solution. The pellet was suspended in L15 complete medium (Gibco); 25 ml FBS (Gibco, Gaithersburg, MD), 10 ml 1 M HEPES (Sigma) and 5 ml penicillin/streptomycin (Sigma) into 470 ml L15 (Gibco), were stacked onto a gradient composed of 12.5% and 28% Percoll (GE Healthcare, Chalfont St Giles, UK). Cells were then further dissociated mechanically and centrifuged at a speed of 1000 rcf at a temperature of 4 °C for 10 min. Neurons segregates between the two Percoll layers were collected and plated at a density of approximately 1.0×10^3 cells on Poly-D-lysine (Becton Dickinson, Franklin Lakes, NJ, USA) and Laminin (Sigma) coated cell culture plates with F12 medium, the coating duration was 2 h prior to cell seeding; 445 ml F12 culture medium (Gibco), 50 ml FBS (Gibco) and 5 ml penicillin/streptomycin (Sigma). Cultures were then placed in a humidified atmosphere of 95% air, 5% CO_2 at a temperature of 37 °C. After seeding, the laser irradiation was performed after 12 h of seeding. Microscopic imaging was performed after 6 h of laser irradiation. The laser irradiation and imaging procedure were repeated at the same time of a day for three days.

2.3. TG Neurons Irradiation Setup with a Near-Infrared Laser

The optical system consisted of a function generator (BK4052-ND, B &K Precision Corporation, Yorba Linda, California, USA), multi-mode fiber (MF22L1, Core diameter: 200 ± 10.0 μm, Cladding diameter: 290 ± 10.0 μm, Thorlabs Inc., Newton, New Jersey, USA), a convex lens, and an aperture with diameter of 17 mm as shown in Fig. 2. A NIR laser with a wavelength of 808 nm, the output power of 500 mW, power-adjustable, and multimode was used to stimulate TG neurons

(a)

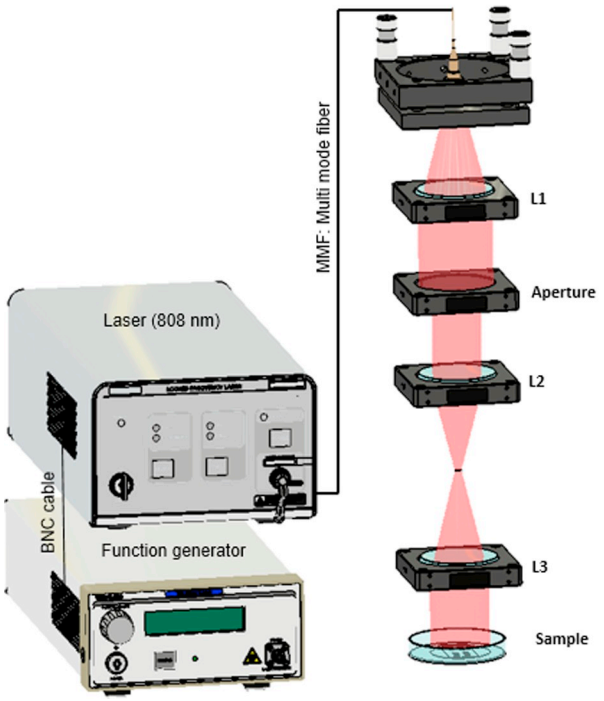

(b)

Parameter	Value			
Pulse frequency (Hz)	0 (CW)	1	10	100
Pulse duration (msec)	∞	500	50	5
Illumination duration (sec)	Laser mode \ Energy density	1 J/cm²	2 J/cm²	10 J/cm²
	CW	40	80	400
	PW	80	160	800

(c)

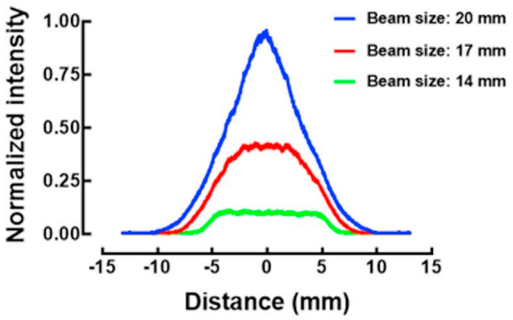

Fig. 2. Schematic diagram of the near-infrared irradiation on *in vitro* cell culture plate. (a) the laser irradiation mode (CW or PW) can be select by a function generator, and the collimated beam irradiated into the well plate containing TG neurons. (b) shows the table list of specific parameters to stimulate TG neurons. We applied four different laser modes (CW and PW mode with 1, 10, and 100 Hz frequency) to compare morphological TG neurons growth differences. For PW mode, the duty cycle was 50%. (c) Beam profile using the equation which is $U_p(Z) = \Delta E_{FWHM} / E_{max}$. The total distance between the laser fiber output and well plate with cells was 36.8 cm. L1: 1-in. convex lens with 25.4 mm focal lengths, Variable aperture: pinhole with 17 mm diameter, L2: 1-in. convex lens with 25.4 mm focal length, and L3: 2-in. convex lens with 100 mm focal length.

through the multimode fiber and lenses with a laser power supply (SDL-808-LM-500MFL, Shanghai Dream Lasers Technology CO., Ltd., Song Jiang, China). We used power density of 25 mW/cm^2 with the beam covered area (2.27 cm^2) to improve the growth of neurons [29]. The measured power delivered onto the dish with cells was 56.8 mW. To make the beam more uniformly, we measured the beam profile by a beam profiler (Spiricon, Ophir Photonics, Jürgen Reingruber, Germany) in Fig. 2c. Eq. (1) is the governing equation for calculation of beam plateau uniformity.

$$U_p(Z) = \Delta E_{FWHM}/E_{max} \quad (1)$$

ΔE_{FWHM} is the full-width at half-maximum (FWHM) of the peak near E_{max} of the power/energy density histogram N (E_i), *i.e.*, the number of (x, y) locations at which a given power/energy density E_i is recorded. Note that plateau uniformity range is zero to one ($0 < U_p(z) < 1$). If the plateau uniformity converges to zero ($U_p(z) \rightarrow 0$) as distributions become more flat-topped. The smaller beam size with variable aperture provides more uniform beam distribution. The output power with the minimum beam size of 14 mm is too low than the output power necessary for optimal laser irradiation. The beam size of 17 mm provides enough output power and reasonable beam uniformity in Fig. 2c.

Using an external function generator, we can change the laser mode from CW to PW mode. In PW mode, we changed the laser pulse frequency with the same energy density to compare the neurite growth effect. Each energy density was set by varying the irradiation time and fix the power density. Thus, the irradiation time was set for 40 s for 1 J/cm^2 with CW, 80 s for 2 J/cm^2 with CW, 400 s for 10 J/cm^2 with CW, while PW took twice the time than that of CW with fixed 50% duty cycle. Laser stimulation was applied daily at the same time on three consecutive days on the well plate containing TG neurons, with the first irradiation at 18 h after seeding the TG neurons.

2.4. Fluorescence Imaging for the Analysis of TG Neuronal Growth with PBM

Fluorescence and bright-field images of the cultured cells were captured to measure the neurite growth of TG neurons using a sCMOS camera (Dhyana 95, Tucsen, Fujian, P. R. CHINA) attached to the inverted microscope with a 10× objective (CPlanN, NA 0.25, Olympus, Shinjuku, Japan) in Fig. 3. For microscopic imaging, culture plates were kept in a stage-top cell incubator system (FC-5 N/Chamlide, Live cell instrument, Seoul, Korea) to maintain a constant temperature and high humidity for the growth of tissue culture cells under the 95% air and 5% CO_2 atmosphere. We used a scientific CMOS camera for 2048 by 2048 pixels with an exposure time of 5 s in fluorescence image and 50 milliseconds in the bright-field image.

2.5. Overall Algorithm to Measure Morphological TG Neuronal Growth

We measured the neurite length, intersections, and enclosing radius of a neuron. These analyses were applied after converting the raw images into skeletonized images. The “Measure Skeleton Length” algorithm is a macro function that calculates the skeleton length by counting pixels in a skeletonized image in ImageJ. The length was measured using a unit of 1-pixel width and height and converted to a micrometer for real scale. Sholl analysis is a broadly used method to quantify the complexity of dendritic arbors by counting the intersections [30]. A line was drawn from the soma to a distant dendrite tip for setting the range to create concentric circles. Following the completion of this process, the number of point where the concentric circles and dendrite meet as counted to identify the intersection. All Sholl analyses were carried out at 1 μm interval steps to a maximum radius of, ~200 μm. We also analyzed the information about the “Enclosing radius” by applying the Sholl analysis. It indicates the last intersecting

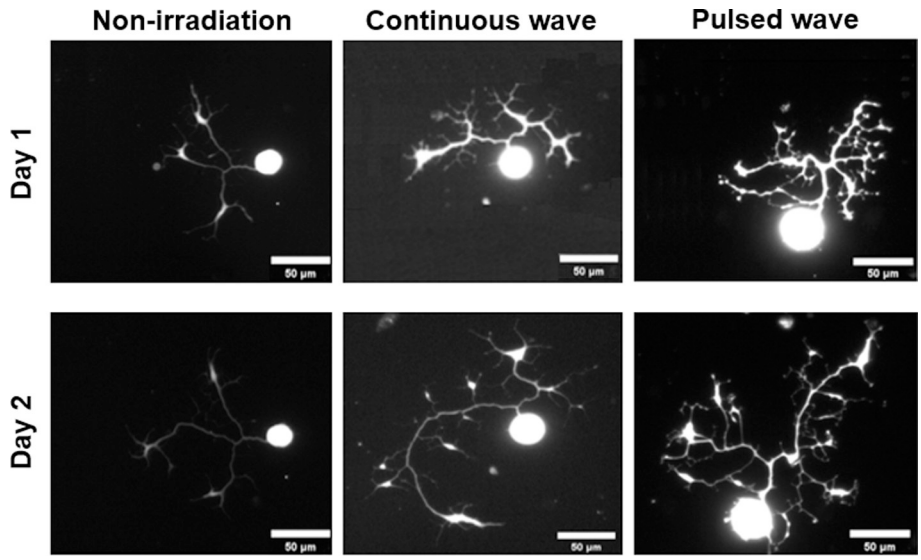

Fig. 3. The representative image in day 1 and day 2 depending on laser mode (continuous wave or pulsed wave) with the same irradiation power. Fluorescence images were obtained by inverted microscope. Energy density of 2 J/cm^2 was used as an example.

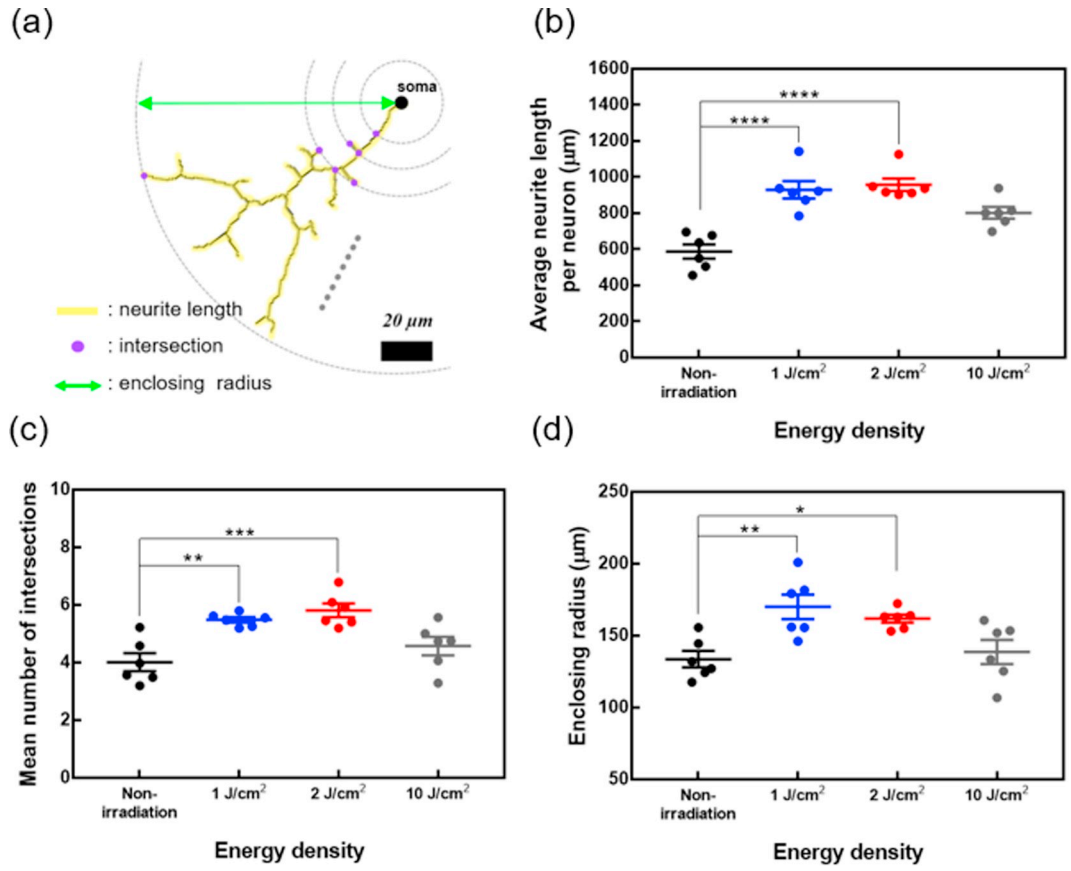

Fig. 4. Comparison of neurite growth between a non-irradiation group and irradiation groups with the CW mode depending on energy density. (a) Representative image of neuron to which the analysis methods were applied, (b) Average neurite length per neuron, (c) Mean number of intersections, (d) Enclosing radius. Data are mean ± S.E.M. (n = 6; *P < .05, **P < .01, ***P < .001, ****P < .0001; *n.s.*,not significant; one-way ANOVA followed by Tukey's multiple comparisons test.

radius, and we can therefore find how far the neurons have sprouted. Using this technique, we can provide the distribution of intersection according to the distance from the soma.

3. Results

In this study, we measured the effect of NIR laser on neurite growth of TG neurons between the non-irradiation group and irradiation groups. For morphological analysis, three analysis methods were applied to the skeletonized image of a neuron in Fig. 4a. While the average neurite length of TG neurons with non-irradiation group, in terms of standard error of the mean, was 587.96 ± 39.87 μm, and the average neurite length for irradiation group with CW mode groups corresponding to energy density of 1, 2, and 10 J/cm^2 were

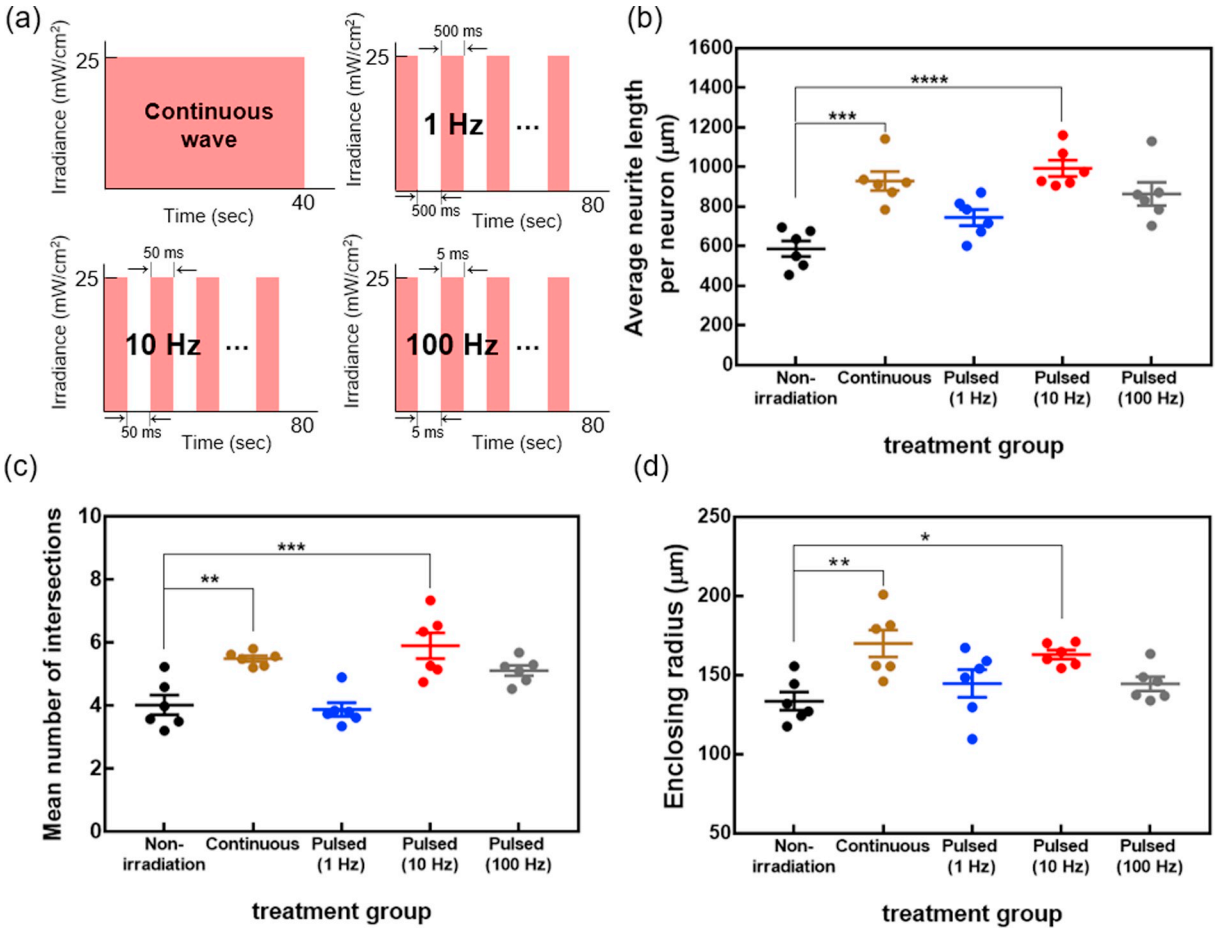

Fig. 5. Comparison of neurite growth between the non-irradiation group and irradiation groups with energy density of 1 J/cm^2 in the CW mode and PW mode depending on frequency. (a) Example of each laser mode and each frequency in the energy density of 1 J/cm^2 (b) Average neurite length per neuron (c) Mean number of intersections (d) Enclosing radius. Data are mean ± S.E.M. (n = 6; *P < .05, **P < .01, ***P < .001, ****P < .0001; *n.s.*,not significant; one-way ANOVA followed by Tukey's multiple comparisons test.)

929.85 ± 48.13 μm, 957.88 ± 34.52 μm, 802.37 ± 32.51 μm, respectively in Fig. 4b. We also measured the mean number of intersections of non-irradiation and irradiation groups with different energy density at 1, 2, and 10 J/cm^2 in Fig. 4c. The mean number of the intersection of TG neurons was at 4.01 ± 0.31 for the non-irradiation groups. In irradiation groups, the mean number of intersections of TG neurons with three different energy densities (1, 2, and 10 J/cm^2) were 5.49 ± 0.09, 5.82 ± 0.24, and 4.58 ± 0.32. The mean number of intersections in irradiation groups with CW mode (1 and 2 J/cm^2) was significantly increased similarly with the averaged neurite length of TG neurons. We measured the enclosing radius of TG neurons in the irradiation group with CW mode at energy density of 1, 2, and 10 J/cm^2. The irradiation groups with 1 and 2 J/cm^2 have increased the enclosing radius of TG neurons compared with non-irradiation group in Fig. 4d. The enclosing radius in 1 and 2 J/cm^2 were 170.06 ± 8.47 μm and 161.85 ± 2.82 μm, respectively. We found that irradiation groups with CW mode in 1 and 2 J/cm^2 significantly increased the neurite growth in terms of the length and complexity compared with the non-irradiation group. However, the neurite growth of the irradiation groups with the energy density of 10 J/cm^2 was less effective than 1 and 2 J/cm^2.

Next, we compared the CW mode with PW mode at several pulse frequencies of 1, 10, and 100 Hz with energy densities of 1, 2, and 10 J/cm^2, respectively in Figs. 5, 6, and 7. A schematic diagram of a CW mode and three PW modes of laser irradiation with x-axis as time (sec) and y-axis as the irradiance (mW/cm^2) in Fig. 5a, 6a, and 7a. We found that neurite growth of both laser modes in energy density of 1 and 2 J/cm^2 were significantly increased compared with that of non-irradiation group. Especially, the neurite growth of irradiation group in energy density of 1 and 2 J/cm^2 with frequency at 10 Hz were more prominent than other frequencies using three types of analysis such as average neurite length, mean number of intersections, and enclosing radius. However, no significant difference was found between the non-irradiation group and the irradiation groups with 10 J/cm^2. Although both the CW and the PW mode at 10 Hz had greater effects than non-irradiation group, there was no statistical difference between CW and PW mode with frequency at 10 Hz in our experimental condition.

4. Discussions

Our approach delineated that PBM with 808 nm on the primary TG neurons facilitates neurite growth *in vitro*. The most effective energy density for PBM on TG neurons was found 1–2 J/cm^2 in both CW and PW modes. Photobiomodulation activates mitochondrial biogenesis. It was previously shown that the local production of ATP promoted distal axonal growth [31]. Thus, laser irradiation on the cells can promote neuronal growth by activating cell metabolism. With NIR irradiation on the cell, cytochrome C oxidase (CCO) in the mitochondria absorbs the photons as photo-acceptors [32]. Photons dissociate nitric oxide (NO) which has been combined with CCO [33,34]. When combined with the CCO, NO serves to inhibit electronic transmission [35]. Thus, the activation of the CCO by the dissociation of NO induces the facilitation of the electron transport chain, resulting in more ATP production [36–38]. In addition, reactive oxygen species (ROS) are generated with NIR irradiation [39]. ROS generated from low energy densities acts as a

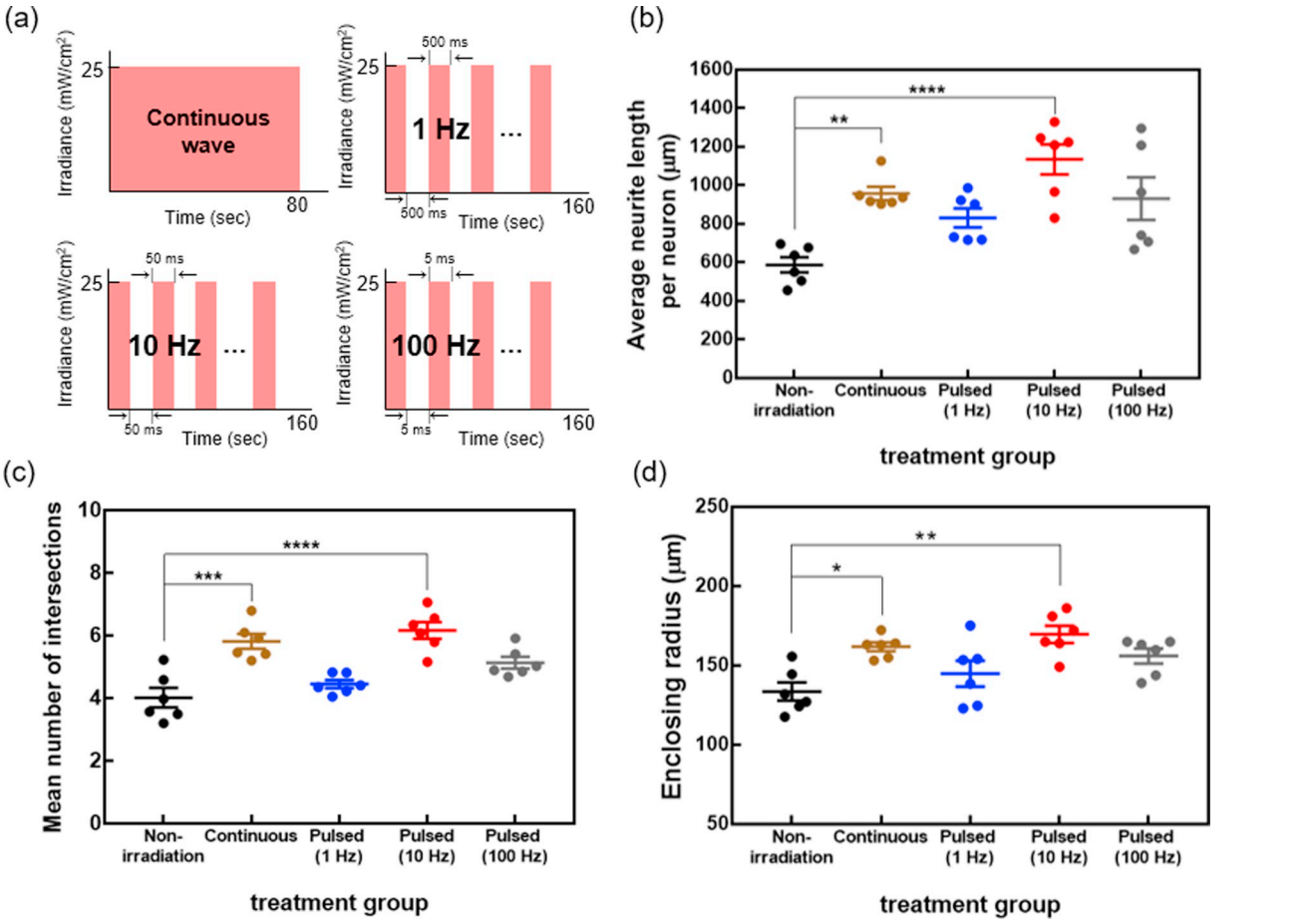

Fig. 6. Comparison of neurite growth between a non-irradiation group and irradiation groups with energy density of 2 J/cm^2 in the CW mode and PW mode depending on frequency. (a) Example of each laser mode and each frequency with energy density of 2 J/cm^2 (b) Average neurite length per neuron (c) Mean number of intersections (d) Enclosing radius. Data are mean ± S.E.M. (n = 6; *P < .05, **P < .01, ***P < .001, ****P < .0001; *n.s.*,not significant; one-way ANOVA followed by Tukey's multiple comparisons test.)

second messenger, serving as a primary signal promoting the NF-kB pathways. However, laser irradiated at higher doses may produce excessive amounts of ROS and can result in the activation of the cellular apoptotic pathways [40]. In this regards, our result shows a similar tendency that laser irradiation with relatively low energy density of 1–2 J/cm^2 results in further neurite growth of TG neurons, especially at 10 Hz frequency, unlike high energy density of 10 J/cm^2 as shown in Figs. 5, 6, and 7. However, recent studies revealed that even higher fluence biomodulated mitochondrial activity with mitochondria purified from bovine liver [41,42]. Thus, further study would be necessary to clarify the biological effect of fluence in photobiomodulation.

We found the most effective frequency for the neurite growth of TG neurons was at 10 Hz. Other groups raised a potential resonance between the frequency of the pulsed wave and the brain wave. In particular, the oscillation of the brain wave having with a rhythm of 4 to 10 Hz may be related to pulsed mode with specific frequency. Ten Hertz pulsed wave laser treatment could result in positive resonance between the frequency of laser and the electrical activity of neurons [43]. However, further research is required to see if the resonance effect can explain the advantages of pulsed wave as the current study was performed *in vitro*. Another possible mechanism for the benefit of pulsed wave with 10 Hz is the pulse duration of 50 milliseconds with 50% duty cycle is similar to some biological time scales. For example, the period could be the half-life of the ion channel in the mitochondrial membrane or another membrane of the cell that reacts with the light [44,45].

Recently, PBM has been widely studied to enhance neuronal activity and growth in the brain, spinal cord, and stem cells [46,47]. Our study identified the neurite growth of TG neurons by both CW mode and PW mode PBM for the first time, and we found the optimal energy density and frequency of NIR irradiation. However, clinical application of our *in vitro* finding needs further investigation. As TG neurons are widely distributed deep inside the face, the delivery of PBM might be challenging while NIR is known for deep tissue light penetration into the tissue.

In vitro experiment with NIR laser is carried out by storing the cells in the media for measurement of neurite growth. Because biological tissues are composed of several components which are water, oxyhemoglobin, deoxyhemoglobin, myoglobin melanin, *etc.* Hemoglobin and melanin absorb the light energy at wavelengths shorter than 600 nm, while wavelengths longer than 970 nm are absorbed by water. The range of red to NIR spectrum (600–1100 nm) can penetrate deeper than the other spectrum. Additionally, 808 nm was shown to provide positive effects on the neuronal growth in the peripheral nervous system [48,49]. Thus, we used wavelengths of 808 nm for our study.

On the other hand, we measured the intersection number which indicates the dendritic complexity of neurons as shown in Figs. 5, 6, and 7. The relationship of neuronal morphology and function and its importance has been recognized for over a century [50–52]. The functionality and morphology of neurons can therefore be used for the diagnosis and treatment in neurological disorders. Increase of dendritic complexity of TG neurons indicates the enhancement of neuronal activity. In addition, intersection number can be interpreted to functional activity such as axon abundance, neuronal co-activity, and synaptic connections [53–55]. Thus, the analysis of the intersection may be used

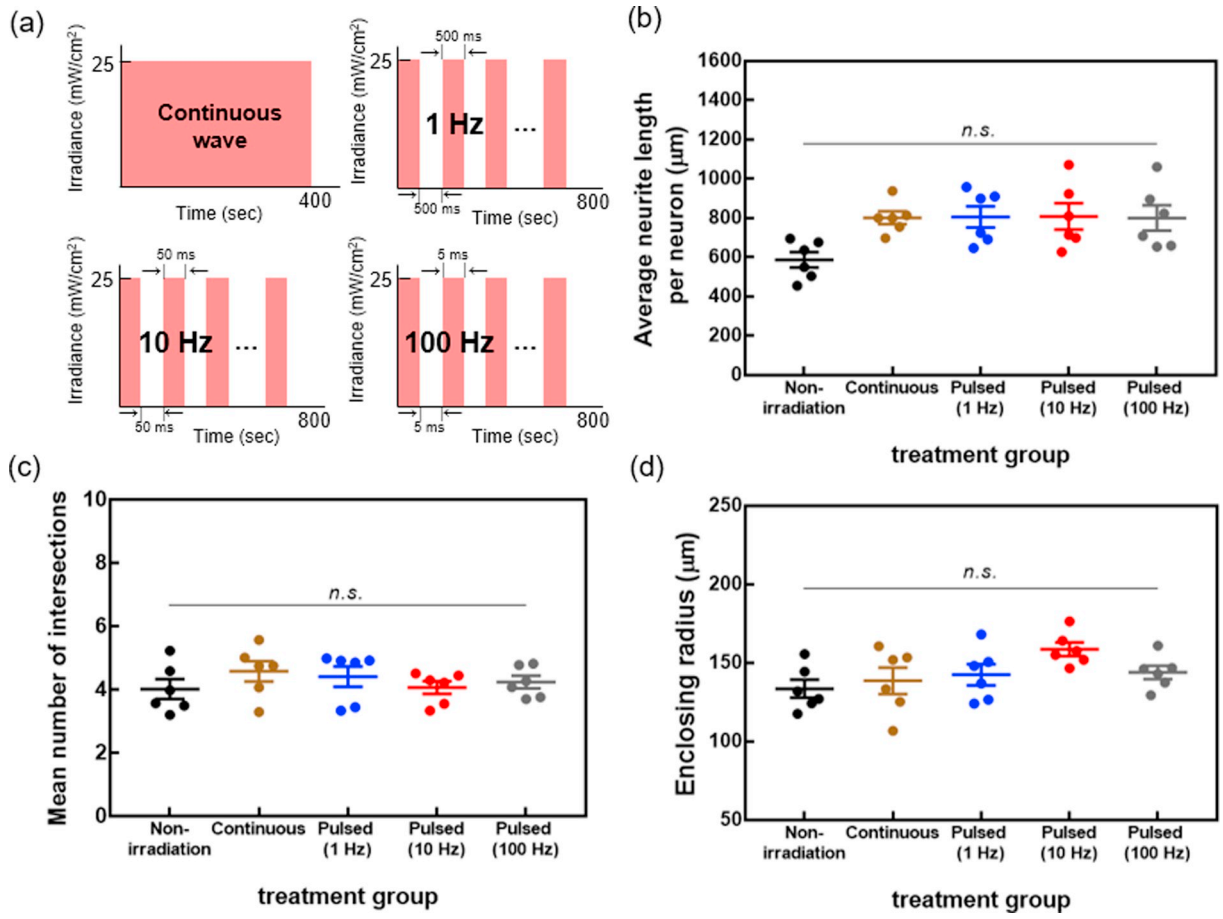

Fig. 7. Comparison of neurite growth between a non-irradiation group and irradiation groups with energy density of 10 J/cm^2 in the CW mode and PW mode depending on frequency. (a) Example of each laser mode and each frequency with energy density of 10 J/cm^2 (b) Average neurite length per neuron (c) Mean number of intersections (d) Enclosing radius. Data are mean ± S.E.M. (n = 6; *P < .05, **P < .01, ***P < .001, ****P < .0001; *n.s.*,not significant; one-way ANOVA followed by Tukey's multiple comparisons test.)

as a functional indicator for neuronal growth. However, it would be necessary to verify the direct relationship between the intersection number and functional analysis for the TG neurons in the future.

While we measured neurite length, the mean number of the intersection, and enclosing radius of TG neurons in response to NIR PBM in the current study, further mechanistic investigation at the molecular and cellular level would provide more insight into the effect of PBM with different irradiation modes. Also, TG neuronal growth with potential *in vivo* setting would provide more relevant results useful for solving clinical problems such as pain relief and dry eye disease related to sensory abnormalities due to nerve cell damages [56,57]. In summary, our research supports the therapeutic potential of PBM *in situ*ations requiring regeneration of the damaged TG neurons.

5. Conclusion

In this study, we developed an optical setup to stimulate the cultured primary trigeminal ganglion neurons from the *Thy1*-YFP transgenic mouse model, demonstrated neurite growth of trigeminal ganglion neurons with 808 nm near-infrared light irradiation, and compared various conditions which include the continuous and pulsed irradiation modes. The effective photobiomodulation energy density, 1 and 2 J/cm^2, and frequency, 10 Hz, were found to promote neuronal growth of trigeminal ganglion neurons. This new investigation could help develop better potential therapeutic approaches to stimulate peripheral nerve regeneration after injury.

Declaration of Competing Interest

The authors declare that they have no known competing financial interests or personal relationships that could have appeared to influence the work reported in this paper.

Acknowledgment

The authors appreciate professor Sang-Mok Lee from HanGil Eye Hospital, Catholic Kwandong University College of Medicine for teaching us the *in vitro* primary culture of trigeminal ganglion neurons and professor Hyuk-Sang Kwon from GIST for helpful discussions throughout the project. This work was supported by Gwangju Institute of Science and Technology (GIST) Research Institute (GRI) grant funded by the GIST in 2020 and grants from the National Research Foundation of Korea (NRF) funded by the Korean government (MEST) (NRF-2019M3C7A1044964), the Brain Research Program through the NRF funded by the Ministry of Science, ICT & Future Planning (NRF-

2017M3C7A1044964), and by the Bio & Medical Technology Development Program of NRF funded by the Korean government (MSIP & MOHW) (NRF-2015M3A9E2030125).

References

[1] S. Graff-Radford, R. Gordon, J. Ganal, S. Tetradis, Trigeminal neuralgia and facial pain imaging, Curr. Pain Headache Rep. (6) (2015) 19, , https://doi.org/10.1007/s11916-015-0495-y.

[2] T. Renton, H. Janjua, J.E. Gallagher, M. Dalgleish, Z. Yilmaz, UK dentists' experience of iatrogenic trigeminal nerve injuries in relation to routine dental procedures: why, when and how often? Br. Dent. J. 214 (12) (2013) 633–642, https://doi.org/10.1038/sj.bdj.2013.583.

[3] T. Renton, A. Dawood, A. Shah, L. Searson, Z. Yilmaz, Post-implant neuropathy of the trigeminal nerve. A case series, Br. Dent. J. 212 (11) (2012), https://doi.org/10.1038/sj.bdj.2012.497.

[4] H. Iro, K. Bumm, F. Waldfahrer, Rehabilitation of the trigeminal nerve, GMS current topics in otorhinolaryngology, head and neck surgery 4 (2005) Doc12.

[5] P.J. Goadsby, Trigeminal autonomic cephalgias (TACs), Acta Neurol. Belg. 101 (1) (2001) 10–19, https://doi.org/10.1201/noe1850705475.ch6.

[6] M.H. Dastjerdi, R. Dana, Corneal nerve alterations in dry eye-associated ocular surface disease, Int. Ophthalmol. Clin. 49 (1) (2009) 11–20, https://doi.org/10.1097/IIO.0b013e31819242c9.

[7] S.E. Wilson, R. Ambrósio, Laser in situ keratomileusis-induced neurotrophic epitheliopathy, Am J. Ophthalmol. 132 (3) (2001) 405–406, https://doi.org/10.1016/S0002-9394(01)00995-3.

[8] G.R. Nettune, S.C. Pflugfelder, Post-LASIK tear dysfunction and dysesthesia, Ocular Surf. 8 (3) (2010) 135–145, https://doi.org/10.1016/S1542-0124(12)70224-0.

[9] G.A. Rocha, A. Acera, J.A. Durán, Laser in situ keratomileusis flap necrosis after trigeminal nerve palsy, Arch. Ophthalmol. 125 (10) (2007) 1423–1425, https://doi.org/10.1001/archopht.125.10.1423.

[10] T. Tölle, E. Dukes, A. Sadosky, Patient burden of trigeminal neuralgia: results from a cross-sectional survey of health state impairment and treatment patterns in six European countries, Pain Pract. 6 (3) (2006) 153–160, https://doi.org/10.1111/j.1533-2500.2006.00079.x.

[11] I.A. Cook, C.P. Kealey, C.M. DeGiorgio, The potential use of trigeminal nerve stimulation in the treatment of epilepsy, Ther. Deliv. 6 (3) (2015) 273–275, https://doi.org/10.4155/tde.14.120.

[12] M. Devor, Neuropathic pain and injured nerve: peripheral mechanisms, Br. Med. Bull. 47 (3) (1991) 619–630, https://doi.org/10.1093/oxfordjournals.bmb.a072496.

[13] C.J. Woolf, R.J. Mannion, Neuropathic pain: aetiology, symptoms, mechanisms, and management, Lancet 353 (9168) (1999) 1959–1964, https://doi.org/10.1016/S0140-6736(99)01307-0.

[14] S. Rochkind, Y. Shapira, Z. Nevo, The potential clinical utility of novel methods for peripheral nerve regeneration: where are we now? Future Neurol. 9 (2) (2014) 105–107, https://doi.org/10.2217/fnl.14.2.

[15] M.M. Mandelbaum-Livnat, M. Almog, M. Nissan, E. Loeb, Y. Shapira, S. Rochkind, Photobiomodulation triple treatment in peripheral nerve injury: nerve and muscle response, Photomed. Laser Surg. 34 (12) (2016) 638–645, https://doi.org/10.1089/pho.2016.4095.

[16] N. Hong, Photobiomodulation as a treatment for neurodegenerative disorders: current and future trends, Biomed. Eng. Lett. 9 (3) (2019) 359–366, https://doi.org/10.1007/s13534-019-00115-x.

[17] K.R. Byrnes, et al., Light promotes regeneration and functional recovery and alters the immune response after spinal cord injury, Lasers Surg. Med. 36 (3) (2005) 171–185, https://doi.org/10.1002/lsm.20143.

[18] J.H. Lee, S. Kim, J.Y. Jung, M.Y. Lee, Applications of photobiomodulation in hearing research: from bench to clinic, Biomed. Eng. Lett. 9 (3) (2019) 351–358, https://doi.org/10.1007/s13534-019-00114-y.

[19] M.R. Hamblin, Shining light on the head: Photobiomodulation for brain disorders, BBA Clin. 6 (2016) 113–124, https://doi.org/10.1016/j.bbacli.2016.09.002.

[20] F. Salehpour, J. Mahmoudi, F. Kamari, S. Sadigh-Eteghad, S.H. Rasta, M.R. Hamblin, Brain photobiomodulation therapy: a narrative review, Mol. Neurobiol. 55 (8) (2018) 6601–6636, https://doi.org/10.1007/s12035-017-0852-4.

[21] U. Oron, S. Ilic, L. De Taboada, J. Streeter, Ga-As (808 nm) laser irradiation enhances ATP production in human neuronal cells in culture, Photomed. Laser Surg. 25 (3) (2007) 180–182, https://doi.org/10.1089/pho.2007.2064.

[22] T. Karu, Primary and secondary mechanisms of action of visible to near-IR radiation on cells, J. Photochem. Photobiol. B Biol. 49 (1) (1999) 1–17, https://doi.org/10.1016/S1011-1344(98)00219-X.

[23] H. Chung, T. Dai, S.K. Sharma, Y.Y. Huang, J.D. Carroll, M.R. Hamblin, The nuts and bolts of low-level laser (light) therapy, Ann. Biomed. Eng. 40 (2) (2012) 516–533, https://doi.org/10.1007/s10439-011-0454-7.

[24] M. Greco, G. Guida, E. Perlino, E. Marra, E. Quagliariello, Increase in RNA and protein synthesis by mitochondria irradiated with helium-neon laser, Biochem. Biophys. Res. Commun. 163 (3) (1989) 1428–1434, https://doi.org/10.1016/0006-291X(89)91138-8.

[25] N. Mochizuki-Oda, Y. Kataoka, Y. Cui, H. Yamada, M. Heya, K. Awazu, Effects of near-infra-red laser irradiation on adenosine triphosphate and adenosine diphosphate contents of rat brain tissue, Neurosci. Lett. 323 (3) (2002) 207–210, https://doi.org/10.1016/S0304-3940(02)00159-3.

[26] L. Andreo, et al., Effects of photobiomodulation on experimental models of peripheral nerve injury, Lasers Med. Sci. 32 (9) (2017) 2155–2165, https://doi.org/10.1007/s10103-017-2359-7.

[27] Y.S. Chen, S.F. Hsu, C.W. Chiu, J.G. Lin, C.T. Chen, C.H. Yao, Effect of low-power pulsed laser on peripheral nerve regeneration in rats, Microsurgery 25 (1) (2005) 83–89, https://doi.org/10.1002/micr.20079.

[28] S.A. Malin, B.M. Davis, D.C. Molliver, Production of dissociated sensory neuron cultures and considerations for their use in studying neuronal function and plasticity, Nat. Protoc. 2 (1) (2007) 152–160, https://doi.org/10.1038/nprot.2006.461.

[29] Y.Y. Huang, K. Nagata, C.E. Tedford, M.R. Hamblin, Low-level laser therapy (810 nm) protects primary cortical neurons against excitotoxicity in vitro, J. Biophotonics 7 (8) (2014) 656–664, https://doi.org/10.1002/jbio.201300125.

[30] K.E. Binley, W.S. Ng, J.R. Tribble, B. Song, J.E. Morgan, Sholl analysis: a quantitative comparison of semi-automated methods, J. Neurosci. Methods 225 (2014) 65–70, https://doi.org/10.1016/j.jneumeth.2014.01.017.

[31] Z.H. Sheng, The interplay of axonal energy homeostasis and mitochondrial trafficking and anchoring, Trends Cell Biol. 27 (6) (2017) 403–416, https://doi.org/10.1016/j.tcb.2017.01.005.

[32] T.I. Karu, Multiple roles of cytochrome c oxidase in mammalian cells under action of red and IR-A radiation, IUBMB Life 62 (8) (2010) 607–610, https://doi.org/10.1002/iub.359.

[33] R.O. Poyton, K.A. Ball, Therapeutic photobiomodulation: nitric oxide and a novel function of mitochondrial cytochrome c oxidase, Discov. Med. 11 (57) (2011) 154–159.

[34] W.P. Hu, J.J. Wang, C.L. Yu, C.C.E. Lan, G.S. Chen, H.S. Yu, Helium-neon laser irradiation stimulates cell proliferation through photostimulatory effects in mitochondria, J. Investig. Dermatol. 127 (8) (2007) 2048–2057, https://doi.org/10.1038/sj.jid.5700826.

[35] W.K. Alderton, C.E. Cooper, R.G. Knowles, Nitric oxide synthases: structure, function and inhibition, Biochem. J. 357 (3) (2001) 593–615, https://doi.org/10.1042/0264-6021:3570593.

[36] T.I. Karu, L.V. Pyatibrat, N.I. Afanasyeva, Cellular effects of low power laser therapy can be mediated by nitric oxide, Lasers Surg. Med. 36 (4) (2005) 307–314, https://doi.org/10.1002/lsm.20148.

[37] D. Pastore, C. Di Martino, G. Bosco, S. Passarella, Stimulation of ATP synthesis via oxidative phosphorylation in wheat mitochondria irradiated with helium-neon laser, Biochem. Mol. Biol. Int. 39 (1) (1996) 149–157, https://doi.org/10.1080/15216549600201151.

[38] S. Passarella, et al., Increase of proton electrochemical potential and ATP synthesis in rat liver mitochondria irradiated in vitro by helium-neon laser, FEBS Lett. 175 (1) (1984) 95–99, https://doi.org/10.1016/0014-5793(84)80577-3.

[39] F. Aimbire, F.V. Santos, R. Albertini, H.C. Castro-Faria-Neto, J. Mittmann, C. Pacheco-Soares, Low-level laser therapy decreases levels of lung neutrophils anti-apoptotic factors by a NF-κB dependent mechanism, Int. Immunopharmacol. 8 (4) (2008) 603–605, https://doi.org/10.1016/j.intimp.2007.12.007.

[40] M.R. Hamblin, Y.Y. Huang, S.K. Sharma, J. Carroll, Biphasic dose response in low level light therapy - an update, Dose-Response 9 (4) (2011) 602–618, https://doi.org/10.2203/dose-response.11-009.Hamblin.

[41] A. Amaroli, S. Ravera, S. Parker, I. Panfoli, A. Benedicenti, S. Benedicenti, An 808-nm diode laser with a flat-top handpiece positively photobiomodulates mitochondria activities, Photomed. Laser Surg. 34 (11) (2016) 564–571, https://doi.org/10.1089/pho.2015.4035.

[42] A. Amaroli, S. Ferrando, S. Benedicenti, Photobiomodulation affects key cellular pathways of all life-forms: considerations on old and new laser light targets and the calcium issue, Photochem. Photobiol. 95 (1) (2019) 455–459, https://doi.org/10.1111/php.13032.

[43] T. Ando, et al., Comparison of therapeutic effects between pulsed and continuous wave 810-nm wavelength laser irradiation for traumatic brain injury in mice, PLoS One 6 (10) (2011), https://doi.org/10.1371/journal.pone.0026212.

[44] T. Priestley, J.A. Kemp, Kinetic study of the interactions between the glutamate and glycine recognition sites on the N-methyl-D-aspartic acid receptor complex, Mol. Pharmacol. 46 (6) (1994) 1191–1196.

[45] B.M. Kampa, J. Clements, P. Jonas, G.J. Stuart, Kinetics of Mg2+ unblock of NMDA receptors: implications for spike-timing dependent synaptic plasticity, J. Physiol. 556 (2) (2004) 337–345, https://doi.org/10.1113/jphysiol.2003.058842.

[46] B. Svobodova, et al., The effect of 808 nm and 905 nm wavelength light on recovery after spinal cord injury, Sci. Rep. 9 (1) (2019), https://doi.org/10.1038/s41598-019-44141-2.

[47] J.C. Heo, J.A. Park, D.K. Kim, J.H. Lee, Photobiomodulation (660 nm) therapy reduces oxidative stress and induces BDNF expression in the hippocampus, Sci. Rep. 9 (1) (2019), https://doi.org/10.1038/s41598-019-46490-4.

[48] Y.J. Chen, et al., Effect of low level laser therapy on chronic compression of the dorsal root ganglion, PLoS One 9 (3) (2014), https://doi.org/10.1371/journal.pone.0089894.

[49] C.C. Medalha, et al., Low-level laser therapy improves repair following complete resection of the sciatic nerve in rats, Lasers Med. Sci. 27 (3) (2012) 629–635, https://doi.org/10.1007/s10103-011-1008-9.

[50] A. Albeg, et al., C. elegans multi-dendritic sensory neurons: morphology and function, Mol. Cell. Neurosci. 46 (1) (2011) 308–317, https://doi.org/10.1016/j.mcn.2010.10.001.
[51] C. Sala, V. Piëch, N.R. Wilson, M. Passafaro, G. Liu, M. Sheng, Regulation of dendritic spine morphology and synaptic function by shank and Homer, Neuron 31 (1) (2001) 115–130, https://doi.org/10.1016/S0896-6273(01)00339-7.
[52] S.F. Tavazoie, V.A. Alvarez, D.A. Ridenour, D.J. Kwiatkowski, B.L. Sabatini, Regulation of neuronal morphology and function by the tumor suppressors Tsc1 and Tsc2, Nat. Neurosci. 8 (12) (2005) 1727–1734, https://doi.org/10.1038/nn1566.
[53] A.D. Bird, H. Cuntz, Dissecting Sholl analysis into its functional components, Cell Rep. 27 (10) (2019) 3081–3096.e5, https://doi.org/10.1016/j.celrep.2019.04.097.
[54] J. Schindelin, et al., Fiji: an open-source platform for biological-image analysis, Nat. Methods 9 (7) (2012) 676–682, https://doi.org/10.1038/nmeth.2019.
[55] T.A. Ferreira, et al., Neuronal morphometry directly from bitmap images, Nat. Methods 11 (10) (2014) 982–984, https://doi.org/10.1038/nmeth.3125.
[56] T. Goto, H. Iwai, E. Kuramoto, A. Yamanaka, Neuropeptides and ATP signaling in the trigeminal ganglion, Jpn. Dent. Sci. Rev. 53 (4) (2017) 117–124, https://doi.org/10.1016/j.jdsr.2017.01.003.
[57] H. Sheha, S. Tighe, O. Hashem, Y. Hayashida, Update on cenegermin eye drops in the treatment of neurotrophic keratitis, Clin. Ophthalmol. 13 (2019) 1973–1980, https://doi.org/10.2147/OPTH.S185184.